Anal. Bioanal. Electrochem., Vol. 8, No. 5, 2016, 629-643

Analytical & Bioanalytical Electrochemistry

2016 by CEE
www.abechem.com

Full Paper

Development of Ni-P Alloy Coatings for Better Corrosion Protection Using Glycerol as Additive

Liju Elias and Amper. Chitharanjan Hegde*

Electrochemistry Research Lab, Department of Chemistry National Institute of Technology Karnataka Srinivasnagar- 575 025, India

*Corresponding Author, Tel.: +8242473201; Fax: +8242474033

E-Mail: acrhegde@gmail.com

Received: 6 April 2016 / Received in revised form: 24 July 2016 / Accepted: 25 July 2016 / Published online: 15 August 2016

Abstract- A new alkaline citrate bath has been formulated for electrodeposition of Ni-P alloy coatings through conventional Hull cell method, using glycerol as an additive. Electrodeposition following induced type of codeposition was carried out on mild steel (MS) substrate at different current densities (c.d.'s), using the basic bath. The influences of bath constituents and operating parameters on the appearance, hardness, thickness and composition of the deposits have been studied. Corrosion behavior of alloy coatings, having hard-adherent mirror bright appearance developed at different c.d.'s were studied by potentiodynamic polarization and electrochemical impedance spectroscopy (EIS) methods in 5 wt.% NaCl solution. Experimental results revealed that corrosion protection efficacy of Ni-P coatings increased with deposition c.d., in proportion of its P content up to an optimal limit, and then decreased. The coating developed at 4.0 A dm^{-2} was found to exhibit the least corrosion rate (14.2×10^{-2} mm y^{-1}), compared to those at other c.d.'s. The process and products of electrodeposition have been studied using different methods, such as cyclic voltammetry (CV), Scanning electron microscopy (SEM), Energy dispersive spectroscopy (EDS) and X-ray diffraction (XRD) analyses. Experimental results were analyzed in the light of principles of induced codeposition and role of additives, and results are discussed.

Keywords- Ni-P alkaline bath, Glycerol, CV study, Corrosion study, SEM and XRD study

1. INTRODUCTION

Alloys of iron-group metals (Fe, Co, and Ni) with other metallic or nonmetallic elements such as P, Mo and W, are widely used in industries owing to their unique properties such as high corrosion resistance [1-3], high hardness [4,5], brilliant luster for decorative purposes [5], electrocatalytic activity for hydrogen evolution [6-8] and interesting magnetic properties [3]. Alloy coatings such as nickel-cobalt (Ni-Co) [9], nickel-tungsten (Ni-W) [1,3,7,10], nickel-phosphorous (Ni-P) [1,4], cobalt-tungsten (Co-W) [1,11] and their ternary or quaternary alloys [12] are being considered to replace conventional hard chromium deposits [13], as they are remarkably hard compared to pure nickel coatings [5]. But the brittleness and the reduced integrity of this alloy deposits, due to transition in material composition and properties across the interface results in the development of stress thereby leading to micro-cracks is also an issue. The mirror-like appearance [4], good corrosion and wear resistance behavior of nickel-phosphorus (Ni-P) alloys making them more attractive and suitable for important technological applications [1,4].

Electrochemical methods such as electroless deposition and electrodeposition are identified as the most practical and inexpensive techniques to synthesize such industrially important iron group alloys [1-11]. It is well known that elements such as P, Mo and W cannot be electrodeposited by themselves independently from solution, whereas, interestingly, this can be deposited as an alloyed element from solutions containing iron-group metals [1,3,5]. This phenomenon is called ‘induced codeposition’ [1-12] as coined first by Brenner. Brenner et al. [5] developed the electrolytes for the electrodeposition of Ni-P and Co-P alloys and classified the codeposition of P with iron-group metals into induced codeposition in order to overcome the shortcomings of electroless Ni-P plating, like use of expensive reducing agent, high operating temperature and difficulty in controlling deposition rate [13,14]. Many research groups thereafter studied the electrodeposition of Ni-P alloy [1,4,5]. Narayan and Mungole [15] proposed the reduction process through hypophosphite to explain the effect of various plating variables in Ni-P alloy deposition. Recently Quanyao et al. [16] reported the synergetic effect of electroless and electrochemical effect on Ni-P alloy development. Further, Sotskaya et al. [17] reported the kinetics of cathodic hydrogen evolution reaction on electrodeposited Ni-P alloy system.

In this paper, electrodeposition resulting in tailored crystallinity and composition of Ni-P alloy has been investigated systematically. Based on the electrochemical study of Ni-P deposition, Ni-P alloy coatings have been deposited with control over the thickness and its composition. An optimal bath has been proposed for the development of good anticorrosive Ni-P alloy coatings. Properties, like hardness, thickness and corrosion behaviors were analyzed as a function of composition and deposition c.d., and the results are discussed.

2. EXPERIMENTAL

2.1. Optimization of Ni-P Bath

Standard Hull cell method was used for the optimization of Ni-P alloy plating bath using Analar grade chemicals ($NiSO_4.6H_2O$, $NaPO_2H_2.H_2O$, NH_4Cl, H_3BO_3 and $C_3H_8O_3$) and double distilled water. The role of current density (c.d.) on coating character has been confirmed by the Hull cell experiments [18,19]. The optimal conditions, in terms of both composition and operating parameters for the development of bright Ni-P alloy on polished mild steel (MS) panels were arrived, and are given in Table 1.

Table 1. The composition and operating parameters of the optimal Ni-P plating bath

Bath constituents	**Composition (per Liter)**	**Operating parameters**
Nickel sulfate hexahydrate ($NiSO_4.6H_2O$)	28.2 g	Anode: Pure Ni
Sodium hypophosphite ($NaPO_2H_2.H_2O$)	51.0 g	Cathode: Mild Steel
Tri-Sodium citrate dihydrate ($Na_3C_6H_5O_7.2H_2O$)	56.2 g	pH: 8.0
Boric acid (H_3BO_3)	20.5 g	Temp: 303 K
Ammonium chloride (NH_4Cl)	10.2 g	Current density range:
Glycerol ($C_3H_8O_3$)	20.0 mL	1.0 A dm^{-2} -6.0 A dm^{-2}

All plating processes were carried out on MS panels at pH=8.0; and the fine tuning of bath pH were made using either H_2SO_4 or NaOH, as required. Prior to plating, the mirror polished MS surface was electro-cleaned, and then pickled in 0.5 M HCl. For comparison purpose all depositions were made in a conventional PVC cell of 250 mL solution capacity; keeping anode and cathode parallel at 5 cm distance for the same duration (600 s). DC power source (Agilent, N6705A) was used as driving force for electrodeposition.

2.2. Characterization

Surface morphology and composition of the coatings were examined using Scanning Electron Microscope (SEM, JSM-7610F from JEOL, USA) and Energy Dispersive Spectroscopy (EDS) analysis tool, respectively. X–ray Diffraction (XRD) signatures, for Ni-P alloy coatings deposited at different c.d.'s were obtained using a JDX–8P (JEOL, Japan), with $CuK\lambda$ radiation (λ=1.5418 A˚) as the X-ray source. The thickness of the deposits was calculated from Faraday's law and was verified using Digital Thickness Tester (Coatmeasure

M&C, ISO–17025). The electrochemical corrosion behavior of the coatings, developed at different c.d.'s (1.0 A dm^{-2} to 6.0 A dm^{-2}) have been tested in 5 wt.% NaCl solution, as representative corrosion medium. Potentiodynamic polarization and electrochemical impedance spectroscopy (EIS) methods were used to evaluate the corrosion behavior of alloy coatings, in a custom made three-electrode cell. All electrochemical potentials referred in this work are with respect to saturated calomel electrode (SCE). Potentiodynamic polarization responses were recorded in a potential ramp of ±250 mV from open circuit potential (OCP), at a scan rate of 1 mV s^{-1}. Impedance behavior was studied at OCP with the voltage perturbation amplitude of 10 mV, in the frequency range from 100 kHz to 10 mHz. All electrochemical studies were carried out at ambient temperature using a computer controlled Potentiostat/Galvanostat (Biologic SP- 150, Biologic Science Instruments, France).

3. RESULTS AND DISCUSSION

3.1. Chemistry of glycerol

Glycerol is a non-toxic, biodegradable, and recyclable liquid that is highly inert, stable and compatible with many other non-toxic and non-irritating chemicals [20]. Further, it facilitates the dissolution of inorganic salts, acids, bases and transition metal complexes hence can be used as a green additive for electroplating. In the case of aqueous plating bath; it is highly miscible with the formation of hydrogen bonds with water molecules and also with free metal ions present in the solution. As the electrode surface is charged, it can get adsorbed on the surface through the electron rich hydroxyl groups, hence, can enhance the adhesion of the coating. Glycerol can interact with the metal surface, metal oxide and deposited metal atoms through its electron-rich hydroxyl groups. The interaction of glycerol at the electrode surface is shown diagrammatically in Fig. 1.

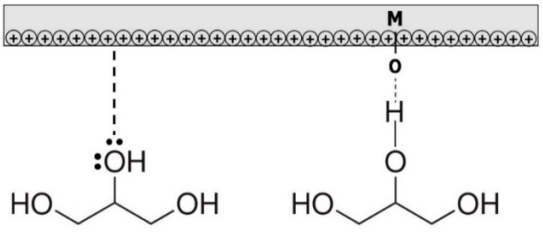

Fig. 1. The plausible mechanism of adsorption of additive onto the metal surface

In fact, glycerol molecules can interact with the alloy coatings through the empty d-orbitals of the transition metal deposits [21], and this property can be exploited to use it as an

additive in electrodeposition, for grain size refinement and formation of smooth and bright coatings.

3.2. Cyclic voltammetry study

Cyclic voltammetry (CV) study of the electrolytic bath has been carried out to understand the effect of added additives on the process and thereby the mechanism of deposition. Cyclic voltammograms obtained at different bath conditions, like: in the absence of any additives, i.e. only with ($NiSO_4$+NH_4Cl+H_3BO_3)=A, (A+$NaPO_2H_2$. H_2O)=B, (B+tri-sodium citrate)=C and with (C+glycerol)=D, at scan rate of 100 mV s^{-1} in a potential window of -2.0 to +2.0 V are shown by curves a, b, c and d, respectively in Fig. 2. It may be observed that the CV curve 'a' in Fig. 2 displays a maximum anodic peak current density in the absenece of any added additive into the bath. It indicates that the Ni coating has lesser stability. However, after addition of the phosphorous salt ($NaPO_2H_2$ H_2O), i.e., a condition corresponding to B, it was found to show two anodic dissolution peaks represented as b_1 and b_2 in the curve 'b' of Fig. 2. It indicates that two anodic peaks are not corresponding to the dissolution of Ni-P alloy of different composition, but of those formed by two different kinetic processes [16,22]. In other words, two peaks are attributed to the formation of Ni-P alloy of different intermetallic phases due to both electrochemical (electroless) and electrolytic deposition [16, 23-25]. Thus, multiple anodic peaks in curve 'b' of Fig. 2 is associated with the dissolution of nickel and phosphorous from various intermetallic phases or solid solutions.

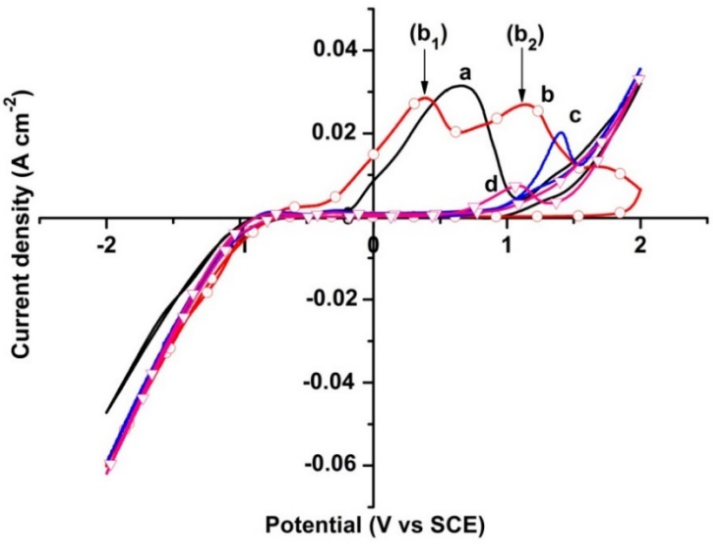

Fig. 2. Cyclic voltammetry study of Ni-P electrolytic bath under different conditions: a) with no additives, i.e. $NiSO_4$+NH_4Cl+H_3BO_3=A, b) A+$NaPO_2H_2$. H_2O=B, c) B+tri-sodium citrate (complexing agent)=C, and d) with C+glycerol (additive)=D (at a scan rate of 100 mV s^{-1}) at 303 K

Under condition C, i.e, in the presence of complexing agent, $Na_3C_6H_5O_7$. $2H_2O$ a single dissolution peak of decreased anodic peak current density (i_{pa}) was observed, as shown by curve 'c' in Fig. 2. It indicates the formation of a single phase Ni-P alloy. Finally, on the addition of glycerol, i.e. condition corresponds to D, the further decrease in i_{pa} value (shown by curve d in Fig. 2) indicating the increased stability of coating after the addition of glycerol. Further, it may be noted that the anodic peak potential has shifted towards more noble side as electrolytic bath condition is changing from A to D. Hence, the successive decrease in i_{pa} and the successive increase in anodic peak potential (E_{pa}) from the conditions of bath A to D demonstrates the role of additives in imparting brightness, homogeneity and electrochemical stability to Ni-P alloy coatings.

Further, to identify the role of additives on mode of mass transport responsible for Ni-P coating characters, the CV study was carried out at different lower scan rates, i.e., 20, 40, 60 and 80 mV s^{-1} corresponding to conditions A, B, C and D. The anodic peak current (i_{pa}) values corresponding to A, B, C and D, were determined from their respective cyclic voltammograms [26]. The scan rate dependence on $i_{pa,}$ under different conditions of the bath is shown in Fig. 3. It is important to note from Fig. 3, that the slopes of plots corresponding to conditions A and D remain almost unchanged. Hence, the chemical constituents corresponding to A and D are responsible for migration and convection mode of the mass transfer process, i.e., adsorption controlled. But greater slope corresponding to B indicates that the complexing agent ($NaPO_2H_2$. H_2O) brings about the diffusion controlled deposition, which is responsible for the formation of various intermetallic phases, affected by increased diffusion of Ni ions towards the cathode. Again under conditions of C, the slope is almost same due to the interaction of additive, leading to a bright, stable and adherent Ni-P coating.

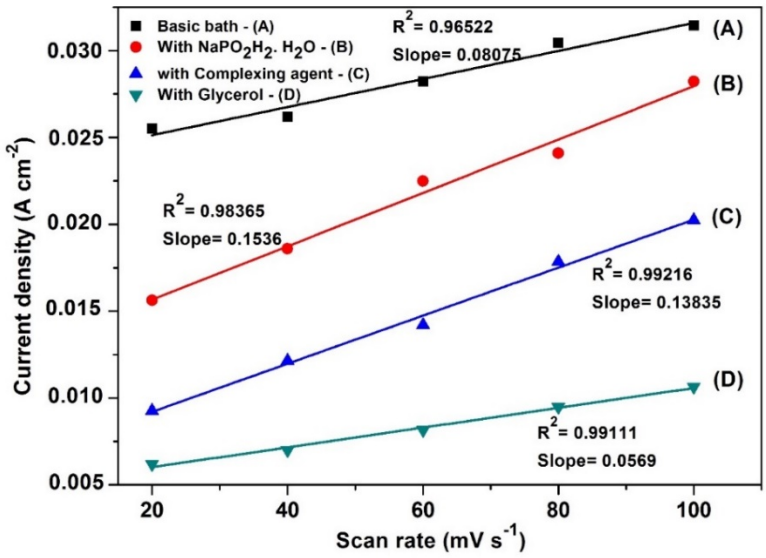

Fig. 3. Scan rate dependency on anodic peak current density (i_{pa}) of Ni-P bath under different conditions (A, B, C and D) at 303 K

3.3. Mechanism of induced codeposition

Phosphorous cannot be electrodeposited as a pure phase, but can be readily co-deposited with iron group metals such as nickel, from solutions containing both Ni and P ions [1,4,5]. It is believed that the strong atomic interaction between Ni and P makes the induced codeposition of Ni-P alloy with stoichiometric composition possible [22]. Even though extensive studies have already been reported on electrodeposition and electroless deposition of Ni-P alloy, most of the deposition were carried out from acid bath, and deposition from alkaline bath are relatively less reported. In this direction, the present study is focused on the deposition of Ni-P alloy from an alkaline citrate bath containing Nickel sulphate and Sodium hypophosphite as the source for Ni and P ions. Tri-sodium citrate has been used as a complexing agent, which along with NH_4Cl can prevent the precipitation of basic salts at higher pH. Boric acid was used as a buffer to maintain the pH, and glycerol as the additive.

From CV study of proposed bath (Table 1), it is clear that the formation of Ni-P alloy coating resulted from the synergistic effect of both electrochemical and electrodeposition process. The characteristic two anodic peaks found in curve 'b' of Fig. 2 indicates that in the presence of sodium hypophosphite (reducing agent), the bath follows both autocatalytic (electroless) and electrolytic deposition of Ni-P alloy [14]. Since the bath can also show deposition of metal onto the substrate through electrochemical reduction of metal ions, i.e., by electroless deposition, the obtained alloy coating is resulted from the synergistic effect of electroless and electrodeposition [16].

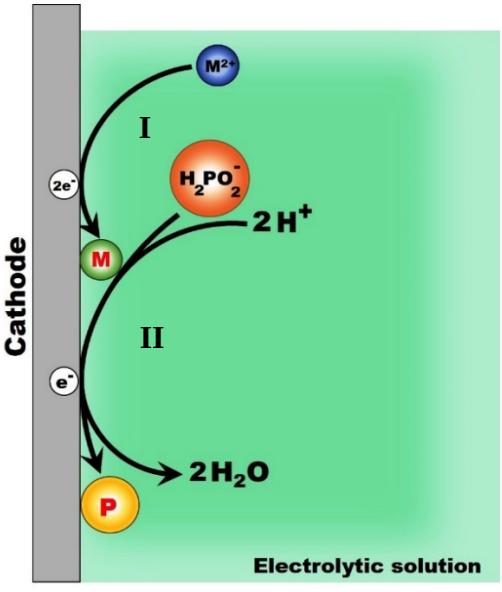

Fig. 4. Mechanism of induced codeposition of Ni-P alloy in the presence of additive

The CV study supports the fact that the proposed Ni-P bath exhibits induced type of codeposition, following the mechanism as shown in Fig. 4. According to which reduction of

Ni^{2+} ion at an active center on the cathode surface takes place, followed by the surface diffusion of the adsorbed Ni atom to a suitable crystal lattice site [15]. The deposited Ni can induce the reduction and codeposition of phosphorous as shown in Fig. 4. The codeposition of P inhibits the further surface diffusion of Ni atoms and hence the growth of crystal nuclei [5]. With increasing P content in the deposit, the rate of fresh nucleus formation becomes higher than the rate of growth of existing crystal nucleus leading to the grain size refining [25]. It is already been reported that ammoniacal alkaline Ni-P bath can give crystalline co-deposited alloy coatings with varying P content; and at the same time, amorphous coatings from acid bath [15]. Crystallographic structures or orientations of the Ni-P alloy coatings are also found to be influenced by the amount of P present in the alloy coatings and undergoes transitions from crystalline to nanocrystalline and eventually to an amorphous type with increasing P content [27].

3.4. Properties of electrodeposited Ni-P alloy coatings

3.4.1. Composition and hardness

The compositional analyses of the electroplated Ni-P alloy coatings have been carried out using energy dispersive X-ray (EDX) facility, attached to SEM machine. The experimental results showed that the P content in the deposit increases with deposition c.d., and the variation in P content of the alloy coatings with c.d. are reported in Table 2. Further, the cathode current efficiency (CCE) was also found to be increased with c.d. The variation in CCE and P content in the deposit with c.d. are shown diagrammatically in Fig. 5. The thickness and Vickers microhardness of the deposits were also found to be increased with c.d., as reported in Table 2.

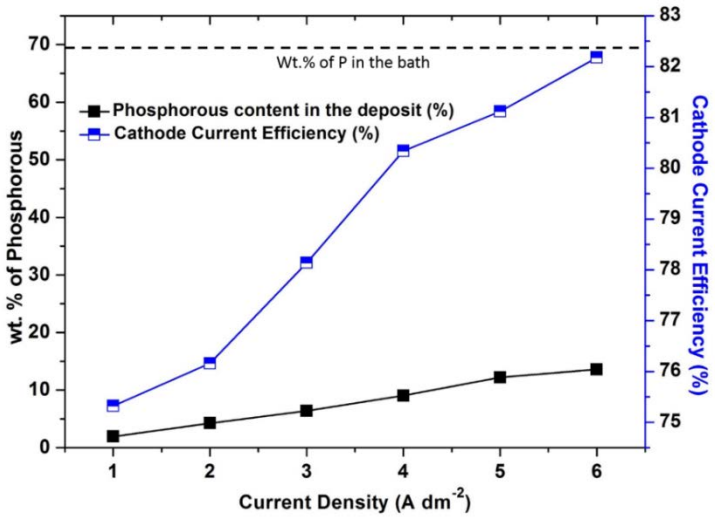

Fig. 5. Effect of c.d. on P content in the deposit and CCE of the bath

Thus, bright and highly adherent Ni-P alloy coatings were developed on MS substrate from optimal bath using known quantities of the direct current (DC). The electrodeposited coatings are tested for their P content, hardness, thickness and corrosion behaviors and the corresponding data are reported in Table 2.

Table 2. Effect of deposition c.d. on the coating characters of Ni-P alloy deposited from optimized bath at 303 K

c.d. (A dm^{-2})	Wt.% of P in deposit	CCE (%)	Vickers micro hardness (V_{100}) (GPa)	Thickness (µm)	$-E_{corr}$ (mV *vs* SCE)	i_{corr} (µA cm^{-2})	CR×10^{-2} (mm y^{-1})	Nature of the deposit
1.0	1.9	75.3	2.34	7.9	551	38.5	40.6	Bright
2.0	4.2	76.1	2.43	11.4	532	29.4	32.8	Bright
3.0	6.3	78.1	2.47	14.1	496	25.3	26.8	Bright
4.0	9.0	80.3	2.67	18.3	513	12.0	14.2	Bright
5.0	12.1	81.1	2.59	19.4	456	17.4	18.7	Bright
6.0	13.5	82.1	2.53	19.8	505	23.0	24.1	Bright

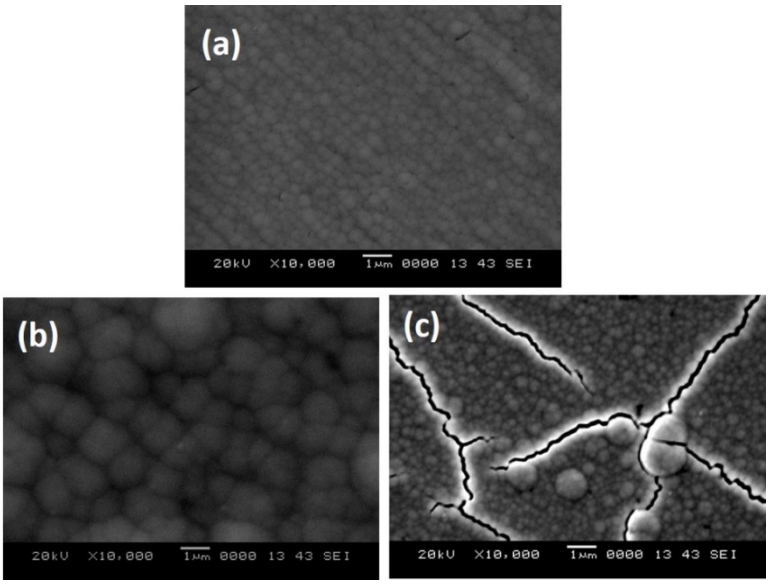

Fig. 6. SEM images of Ni-P alloy coatings deposited at: a) 2.0 A dm^{-2}, b) 4.0 A dm^{-2} and c) 6.0 A dm^{-2}, showing the variation in surface morphology with deposition c.d.

3.4.2. SEM study

The surface appearance of electrodeposited specimens was initially evaluated visually and all specimens were found to be displayed a uniform and satisfactory surface appearance without any pinhole or blisters. Then the surface micrographs of the Ni-P alloy deposits developed at different c.d.'s were obtained using scanning electron microscopy (SEM) as shown in Fig. 6 (only representative). The variation in micrographs with an increase in deposition c.d. is clearly evident from the SEM images given in Fig. 6.

It may be noted that the formation of micro-cracks in Ni-P alloy coatings at high c.d. (6.0 A dm^{-2}) as shown in Fig. 6(c) is attributed to the increase of P content in the deposit, as reported in Table 2. The formation of micro-cracks in the deposits as shown in SEM image (Fig. 6(c)) may be due to the internal stress in the deposits originated from the codeposition of hydrogen, together with Ni-P alloys at higher deposition c.d. It was also found that, with increasing c.d. the deposit is becoming more crystalline with nodular and rough surface, compared to lower c.d. coatings. The surface morphology of the amorphous samples always consists of a very flat surface, while the crystalline structure has a nodular, much rougher surface. These findings are in consistent with the results of Narita et al. [28] on electroplated amorphous and crystalline Ni-S alloys, and of Omi et al. [29] on electroplated Fe-W coatings.

3.4.3. XRD Study

The phase structures of Ni-P coatings at different c.d.'s were assessed by XRD analyses.

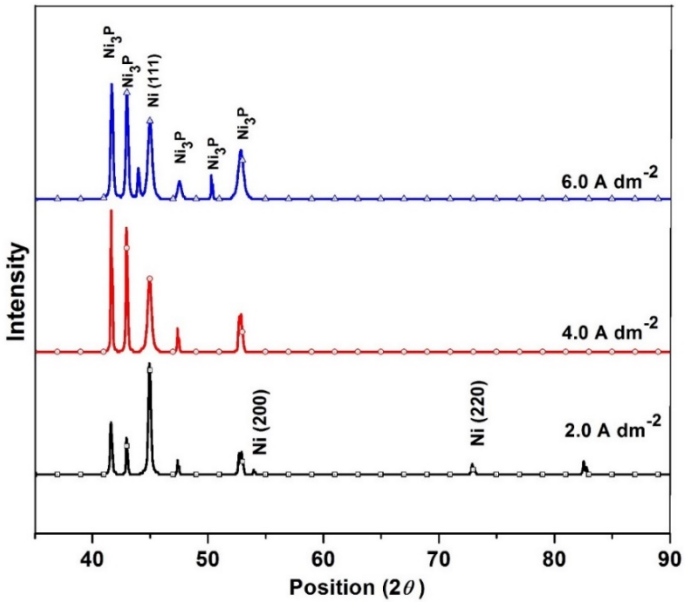

Fig. 7. X-ray diffraction peaks of Ni-P alloy deposited at different c.d.'s from the optimal bath

The XRD patterns of the coatings, corresponding to 2.0, 4.0 and 6.0 A dm^{-2} (only representative) are given in Fig. 7. The obtained diffractogram showing the peaks corresponding to both Ni and Ni_3P confirms the equilibrium existence of the two phases in the deposit. At low P concentrations (4.2 wt.%), i.e., the coating developed at 2.0 A dm^{-2}, the nickel peaks corresponds not only to (111) plane, but also to (200), (220) planes were observed. As the P content increased, the only prominent nickel (111) peak left, and other peaks of nickel started diminishing in intensity, and almost completely disappeared in the diffractogram, at 4.0 and 6.0 A dm^{-2}. On the other hand, with increasing the P content in the deposit, more Ni_3P peaks with increasing intensity was started appearing in the diffraction pattern. At higher c.d., the intensity of Ni_3P peak is observed to be more dominating than Ni (111) peak [15]. Hence, it may be inferred that increased micro-cracks (due to stress) of the coatings at high c.d. is due to the precipitation of Ni_3P grains with an increase in the concentration of P in the deposit [25].

3.5. Corrosion Study

3.5.1. Tafel's polarization study

The corrosion resistance of Ni-P alloy coatings developed at different c.d.'s was evaluated by Tafel's polarization method in 5 wt.% NaCl as corrosion medium. Tafel's extrapolation method was used to measure the corrosion rate [30]. The representative polarization responses of Ni-P alloy coatings are shown in Fig. 8, and the corresponding corrosion data are given in Table 2.

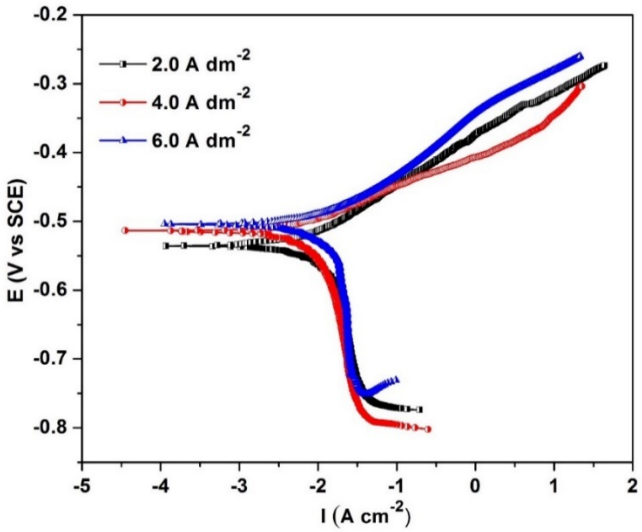

Fig. 8. Potentiodynamic polarization behaviors of Ni-P alloy coatings deposited at different c.d.'s from optimal bath

In Tafel plots, the cathodic reaction corresponds to the evolution of hydrogen; and anodic branch of polarization curve corresponds to the alloy dissolution, and is the deciding factor for corrosion resistance [21,23]. From the corrosion data (Table 2), it may be noted that the corrosion rate (CR) of the coatings were decreased with increase in P content only up to an optimal level (9.0 %) and then increased. From the polarization responses given in Fig. 8, it is clear that the cathodic branch of the plot shows almost similar reaction rate, whereas the anodic branch shows decreased dissolution rate with increase in deposition c.d. up to 4.0 A dm^{-2} (increase in P content up to 9.0%) and then increased.

3.5.2. Electrochemical Impedance measurements

The powerful and non-destructive EIS method has also been used to study the corrosion behavior of Ni-P alloy coatings. The plot of the imaginary impedance component (Z) against the real impedance component (Z') at each excitation frequency, called Nyquist plot of the representative Ni-P alloy coatings is shown in Fig. 9. The interception of frequency responses on the real axis of Nyquist plot at higher frequencies is attributed to the electrolyte bulk resistance (R_s) and at lower frequencies to the polarization resistance or charge transfer resistance (R_{ct}) [31]. Hence, from the nature of Nyquist plots, it may be inferred that Ni-P alloy coating deposited at 4.0 A dm^{-2} as the most corrosion resistant coating than all other coatings.

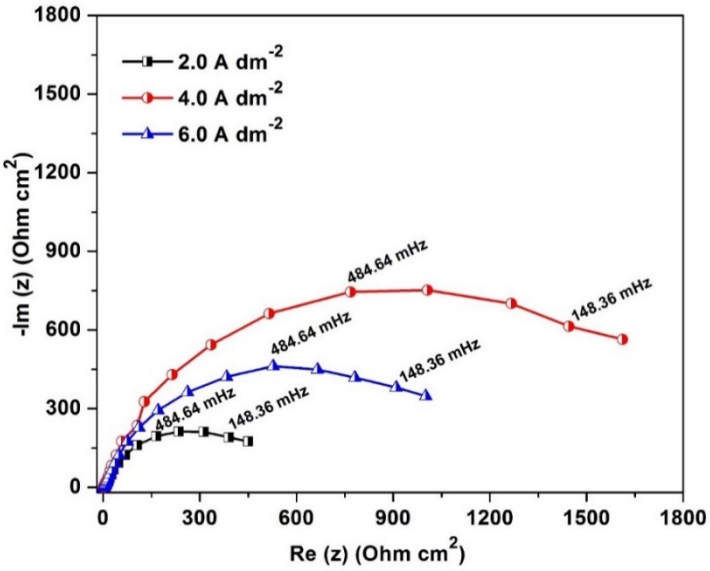

Fig. 9. Nyquist responses for Ni-P alloy coatings deposited at different c.d.'s from the optimal bath, showing variation in R_{ct} values with c.d

Further, the electrode–electrolyte interface of the alloy coatings in the corrosion medium was simulated through electrical equivalent circuit (EEC) fitment. The Nyquist responses pertaining to the alloy coatings developed at different c.d's were analyzed, using $Z_{simpwin}$

software. The fitment plot of optimal Ni-P alloy coating, developed at 4.0 A dm^{-2} is shown in Fig. 10, along with its EEC model (inset). A close agreement was found between the experimentally observed and simulated impedance response as shown in Fig. 10. The value of circuit parameters, like solution resistance (R_s), polarization resistance (R_{ct}) and double layer capacitance/constant phase element (Q), corresponding to all coatings are reported in Table 3. The simulated data corresponding to different c.d.'s, obtained from the same bath further confirms that the coating deposited at 4.0 A dm^{-2} as more corrosion resistant.

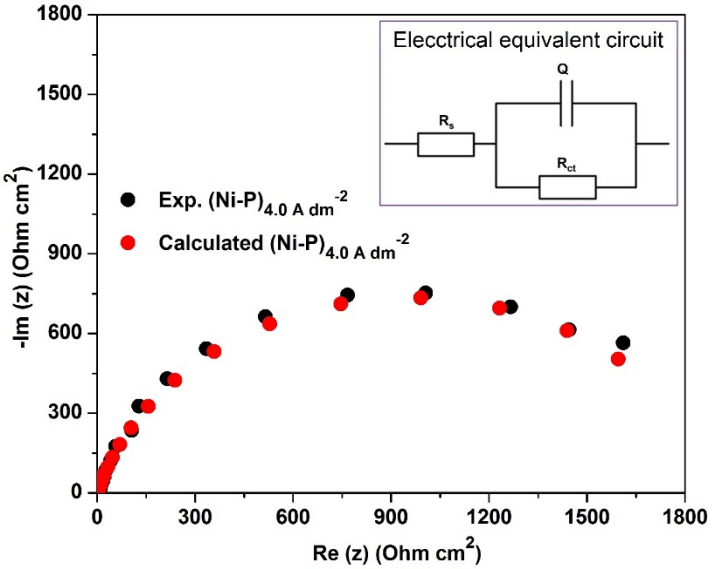

Fig. 10. Electrical equivalent circuit (EEC) fitment for Nyquist response of Ni-P alloy coating developed at 4.0 A dm^{-2} (using $Z_{simpwin}$ software) along with equivalent circuit in the inset

Table 3. The electrochemical parameters of simulated circuit, like solution resistance (R_s), polarization resistance (R_{ct}) and double layer capacitance (Q) corresponding to Ni-P alloy coatings developed at different c.d.'s

Coating configuration	R_s (Ohm)	R_{ct} (Ohm)	Q (µF)
$(Ni\text{-}P)_{1.0\ A\ dm^{-2}}$	1.6	392	324.5
$(Ni\text{-}P)_{2.0\ A\ dm^{-2}}$	1.4	412	294.3
$(Ni\text{-}P)_{3.0\ A\ dm^{-2}}$	1.1	1012	226.6
$(Ni\text{-}P)_{4.0\ A\ dm^{-2}}$	1.1	1468	181.7
$(Ni\text{-}P)_{5.0\ A\ dm^{-2}}$	1.1	1131	214.2
$(Ni\text{-}P)_{6.0\ A\ dm^{-2}}$	1.1	1016	224.8

Thus, the study revealed that the Ni-P alloy coating developed at 4.0 A dm^{-2} as the most protective and decorative one with least CR (14.2×10^{-2} mm y^{-1}), compared to those at other c.d.'s. Hence, Ni-P alloy coating deposited at 4.0 A dm^{-2} has been selected as the optimal coating from the proposed bath.

4. CONCLUSIONS

A new alkaline citrate bath has been optimized for the development of Ni-P alloy coatings using glycerol as the additive. The CV study demonstrated that the addition of both complexing agent and glycerol contributes towards the increased electrochemical stability of the Ni-P alloy coatings. The CCE, thickness, micro-hardness and corrosion resistance of the coatings were found to be increased with c.d. as a function of P in the deposit, in compliance with the general behavior of induced codeposition. Ni-P alloy coating developed at 4.0 A dm^{-2} was found to be the optimal, from the proposed bath, showing the least corrosion rate (14.2×10^{-2} mm y^{-1}).

Acknowledgments

Mr. Liju Elias acknowledges National Institute of Technology Karnataka (NITK), Surathkal, India for financial support in the form of Institute Fellowship.

REFERENCES

[1] S. Sakai, S. Nakanishi, and Y. Nakato, J. Phys. Chem. B 110 (2006) 11944.
[2] T. Akiyama, and H. Fukushima, ISIJ Int. 32 (1992) 787.
[3] M. Donten, H. Cesiulis, and Z. Stojek, Electrochim. Acta 45 (2000) 3389.
[4] T. Mahalingam, M. Raja, S. Thanikaikarasan, C. Sanjeeviraja, S. Velumani, H. Moon, and Y. D. Kim, Mater. Characterization 58 (2007) 800.
[5] A. Brenner, Electrodeposition of Alloys, Academic Press: New York, Vol. 1-2 (1963).
[6] I. Paseka, and J. Velicka, Electrochimica Acta 42 (1997) 237.
[7] L. Elias, K. Scott, and A. C. Hegde, J. Mater. Eng. Perform. 24 (2015) 4182.
[8] T. Burchardt, Int. J. Hydrogen Energ. 26 (2001) 1193.
[9] L. Wang, Y. Gao, Q. Xue, H. Liu, and T. Xu, Appl. Surface Sci. 242 (2005) 326.
[10] L. Elias, and A.C. Hegde, Surface Coatings Technol. 283 (2015) 61.
[11] C. L. Aravinda, V. S. Muralidharan, and S. M. Mayanna, J. Appl. Electrochem. 30 (2000) 601.
[12] A. Saedi, and M. Ghorbani, Mater. Chem. Phys. 91 (2005) 417.
[13] D. T. Gawne, and U. Ma, Surface Eng. 4 (1988) 239.

[14] T. S. N. Sankara Narayanan, and S. K. Seshadri, Electro-and electroless plated coatings for corrosion protection (2008) pp. 177-221.
[15] R. Narayan, and M. N. Mungole, Surface Technol. 24 (1985) 233.
[16] Q. Yu, Z. Zeng, Y. Liang, W. Zhao, S. Peng, Z. Han, G. Wang, X. Wu, and Q. Xue, RSC Adv. 5 (2015) 27242.
[17] N. V. Sotskaya, O. V. Dolgikh, L. V. Sapronova, and Y. G. Kravtsova, Protection of Metals Phys. Chem. 51 (2015) 360.
[18] K. Nasser, Electroplating: Basic principles, processes and practice. Berlin: Atotech Deutschland GmbH (2004).
[19] N.V. Parthasaradhy, Practical Electroplating Handbook, (Retroactive Coverage). Prentice-Hall, Inc. (USA), 1444 (1989).
[20] A. Wolfson, and C. Dlugy, Org. Commun. 2 (2009) 34.
[21] U. P. Kumar, C. J. Kennady, and Q. Zhou, Surface Coatings Technol. 283 (2015) 148.
[22] J. Crousier, Z. Hanane, and J. P. Crousier, Thin Solid Film. 248 (1994) 51.
[23] G. Lu, and G. Zangari, Electrochim. Acta 47 (2002) 2969.
[24] D. R. Gaskell, Introduction to the Thermodynamics of Materials, CRC Press (2008).
[25] A. M. Pillai, A. Rajendra, and A. K. Sharma, J. Coatings Technol. Res. 9 (2012) 785.
[26] J. B. Allen, and R. F. Larry, others, Electrochemical methods: fundamentals and applications, John Wiley & Sons, Inc. (2001) 156–176.
[27] B. Elsener, D. Atzei, A. Krolikowski, and A. Rossi, Surface Inter. Anal. 40 (2008) 919.
[28] A. Narita, T. Watanabe, and Y. Tanabe, Rapidly Quenched Metals, (ed. By S. Steeb and H. Warlimont), Vol 1, North-Holland (1985).
[29] T. Omi, H. Yamamoto, and H. L. Glass, J. Electrochem. Soc. 119 (1972) 168.
[30] H. H. Willard, L. L. J. Merritt, J. A. Dean, and F. A. J. Settle, Instrumental methods of analysis, 7th edition (1988).
[31] E. Barsoukov, and J. R. Macdonald, Impedance spectroscopy: theory, experiment, and applications, John Wiley & Sons (2005).